Temperature shifts of the resonances of the NV⁻ center in diamond

M. W. Doherty,[1,*] V. M. Acosta,[2,†] A. Jarmola,[2] M. S. J. Barson,[1] N. B. Manson,[1] D. Budker,[2,3] and L. C. L. Hollenberg[4]

[1]*Laser Physics Centre, Research School of Physics and Engineering, Australian National University,*
Australian Capital Territory 0200, Australia
[2]*Department of Physics, University of California, Berkeley, California 94720-7300, USA*
[3]*Nuclear Science Division, Lawrence Berkeley Laboratory, Berkeley, California 94720, USA*
[4]*School of Physics, University of Melbourne, Victoria 3010, Australia*
(Received 27 October 2013; revised manuscript received 11 July 2014; published 28 July 2014)

Significant attention has been recently focused on the realization of high precision nanothermometry using the spin-resonance temperature shift of the negatively charged nitrogen-vacancy (NV⁻) center in diamond. However, the precise physical origins of the temperature shift is yet to be understood. Here, the shifts of the center's optical and spin resonances are observed and a model is developed that identifies the origin of each shift to be a combination of thermal expansion and electron-phonon interactions. Our results provide insight into the center's vibronic properties and reveal implications for NV⁻ thermometry.

The negatively charged nitrogen-vacancy (NV⁻) center in diamond [1] is an important quantum technology platform for a range of new applications exploiting quantum coherence. Beyond quantum information processing, the prospect of employing the NV⁻ center as a room temperature nanoscale electric and magnetic field sensor has attracted considerable interest [2–7]. Recently, the effects of temperature on the center's ground state spin resonance have been investigated [8], which enabled the influence of temperature on existing NV⁻ metrology applications to be characterized and new thermometry applications to be proposed [8–11] and demonstrated [12–14]. However, the temperature shift of the center's spin resonance is not well understood and previous attempts at modeling the shift have been largely unsuccessful [8,10,11]. It is evident that the implementation of the NV⁻ center as a nanothermometer, magnetometer, or electrometer requires a thorough understanding of the temperature shifts of its resonances, particularly if these implementations are designed for ambient conditions [15]. Here, the temperature shifts of the center's visible, infrared, and spin resonances are observed and a model is developed that identifies the origin of each shift to be a combination of thermal expansion and electron-phonon interactions. This insight reveals implications for NV⁻ metrology and our model may be generalized to similar defects.

The NV⁻ center is a C_{3v} point defect in diamond consisting of a substitutional nitrogen atom adjacent to a carbon vacancy that has trapped an additional electron [see Fig. 1(a)]. As per Fig. 1(b), the one-electron orbital level structure of the center contains three defect orbitals (a_1, e_x, and e_y) deep within the diamond band gap. Electron paramagnetic resonance (EPR) observations and *ab initio* calculations indicate that these orbitals are highly localized to the center [16–20]. Figure 1(c) shows the center's many-electron electronic structure generated by the occupation of the three orbitals by four electrons

[21,22], including the low-temperature zero phonon line (ZPL) energies of the visible ($E_V \sim 1.946$ eV) [23] and infrared ($E_{IR} \sim 1.19$ eV) [24–26] transitions.

As per the inset of Fig. 1(c), the ground $^3A_2$ level exhibits a zero-field fine structure splitting between the $m_s = 0$ and ±1 spin sublevels of $D \sim 2.88$ GHz (low temperature) due principally to electron spin-spin interaction [27]. While second-order spin-orbit interaction does contribute to the zero-field splitting, its contribution is much smaller than that of spin-spin and it can be ignored in this work [1]. Under crystal strain that distorts the center's C_{3v} symmetry, the $m_s = \pm1$ sublevels are mixed and their degeneracy is lifted. The spin Hamiltonian of the $^3A_2$ level is

$$H = D\left[S_z^2 - S(S+1)/3\right] + \mathcal{E}\left(S_x^2 - S_y^2\right), \quad (1)$$

where $\mathcal{E}$ is the strain parameter, the $S = 1$ spin operators are dimensionless, and the z coordinate axis coincides with the center's C_{3v} symmetry axis [see Fig. 1(a)].

The spin of the ground $^3A_2$ level is optically polarized due to spin-selective nonradiative intersystem crossings (ISC) that preferentially depopulate the $m_s = \pm1$ sublevels and populate the $m_s = 0$ sublevel [1]. The ISC also lead to spin-dependent optical fluorescence that enables the ground state spin to be measured and the performance of optically detected magnetic resonance (ODMR) [1]. The nonradiative ISC of the center are not fully understood, but they are currently believed to be the combined result of spin-orbit coupling of the lowest energy triplet ($^3A_2$,^3E) and singlet ($^1A_1$,^1E) levels and electron-phonon interactions [1].

There were extensive temperature studies of the NV⁻ center conducted at the time of its first identification [28,29]. Davies observed the temperature shifts of the visible ZPL energy accompanied by changes in its homogeneous linewidth and luminescence intensity [28]. Plakhotnik *et al.* similarly studied the temperature dependence of the entire NV⁻ luminescence intensity and its potential for nanothermometry [30]. Davies provided an accurate vibronic model of these temperature effects by considering both the response of the ZPL to the stress induced by thermal expansion of the bulk lattice and electron-phonon interactions at the center. Acosta *et al.* have

*marcus.doherty@anu.edu.au
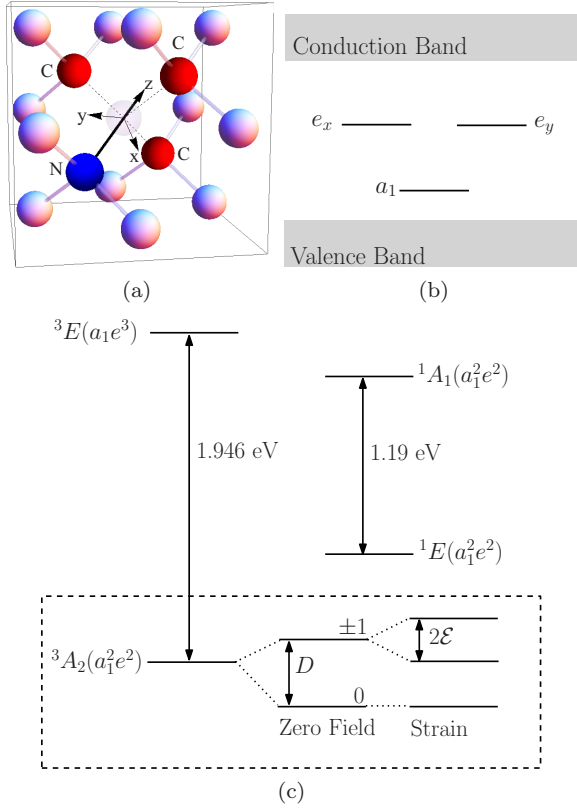†Present address: Googleplex, 1600 Ampitheatre Pkwy., Mountain View, CA 94043.

FIG. 1. (Color online) (a) Schematic of the NV center depicting the vacancy, nearest-neighbor carbon atoms, substitutional nitrogen atom, next-to-nearest carbon neighbors, and the adopted coordinate system (z axis aligned with the center's C_{3v} axis and the x axis within one of the center's mirror planes). (b) The NV^- one-electron orbital level structure depicting the diamond valence and conduction bands and the three defect orbitals (a_1, e_x, and e_y) within the band gap. (c) The center's many-electron electronic structure, including the low-temperature visible $E_V \sim 1.946$ eV and infrared $E_{IR} \sim 1.19$ eV ZPL energies. The electronic configurations of the many-electron levels are indicated in parentheses. Inset: The fine structure of the ground $^3A_2$ level: at zero field with a single splitting $D \sim 2.88$ GHz (low temperature); and under symmetry lowering strain, with an additional strain dependent splitting $2\mathcal{E}$.

studied the temperature dependence of the ground state spin resonance and demonstrated that the temperature shift of D was not consistent with a model based purely on the $\sim \langle 1/r^3 \rangle$ spatial dependence of electron spin-spin interaction and the thermal expansion of the bulk crystal lattice [8,10]. Chen *et al.* [11] later observed that the temperature dependence of the shifts of D and the visible ZPL energy were similar and proposed that the shifts were both due to some local thermal expansion that acted similarly on the center's visible and magnetic transitions. However, Chen *et al.* did not add detail to their hypothesis, thereby leaving the explanation of the temperature shift of D an unresolved problem. To our knowledge, the temperature shift of the infrared ZPL energy has not been reported previously.

Davies' model of the temperature shift of the visible ZPL is equally valid for the shifts of the infrared ZPL and D. The latter follows from the recognition that the spin

transitions of the ground state spin resonance are zero-phonon transitions (i.e., the observed spin resonance is a ZPL). Davies adopts the quasiharmonic approximation to avoid the explicit treatment of vibrational anharmonicity. Instead, the anharmonic displacement of the mean positions of nuclei at higher vibrational quantum numbers is approximated by the static strain of thermal expansion. The anharmonic reduction of vibrational energy level spacings at higher quantum numbers is ignored, such that the vibrational modes remain harmonic and their frequencies are temperature independent.

In Davies' model, there are two contributions to temperature shifts of ZPLs: (1) the electronic energies are perturbed by the strain of thermal expansion, and (2) the vibrational frequencies associated with different electronic levels differ. The latter is a consequence of the vibrational potential-energy functions of the electronic levels having different curvatures. Equivalently, the differences in vibrational frequencies may be described as outcomes of quadratic electron-phonon interactions [28]. Davies' model may be further understood by considering transitions between the vibronic manifolds of two electronic states. Zero-phonon transitions occur between vibronic levels of the electronic states that do not differ in their vibrational quantum numbers. If the initial electronic state is in thermal equilibrium, the observed central ZPL energy is the thermal average of all zero-phonon transition energies.

As temperature increases, the equilibrium positions of the nuclei expand and the electronic energies shift, resulting in a common shift of all of the zero-phonon transition energies, and thus of the ZPL energy. Introducing the mass-weighted nuclear displacement coordinate $Q_{ex}(T)$ of thermal expansion, the relative temperature shift of the electronic energies is

$$\Delta E_{ex}(T) = \left. \frac{\partial \Delta E_{el}}{\partial Q_{ex}} \right|_0 Q_{ex}(T), \tag{2}$$

where the derivative is evaluated at $Q_{ex} = 0$ and $\Delta E_{el} = E_{el,1} - E_{el,2}$ is the difference in electronic energies and $E_{el,i}$ is the electronic energy of the ith electronic state. Since thermal expansion and hydrostatic pressure are intimately related, the contribution of thermal expansion to the ZPL shift is more simply [28]

$$\Delta E_{ex}(T) = A P(T), \tag{3}$$

where A is the hydrostatic pressure shift of the ZPL, $P(T) = B \int_0^T e(t)dt$ is the pressure of thermal expansion, $B = 442$ GPa is the bulk modulus of diamond, and $e(T)$ is the diamond volume expansion coefficient.

If the vibrational frequencies of the two electronic states differ, the energy of a zero-phonon transition will depend linearly on vibrational quantum number. Introducing the vibrational density of modes $\rho(\omega)$ and performing the thermal average, the contribution of electron-phonon interactions to the ZPL temperature shift is

$$\Delta E_{e\text{-}p}(T) = \hbar \int_0^\Omega n(\omega, T)\delta(\omega)\rho(\omega)d\omega, \tag{4}$$

where $n(\omega, T) = (e^{\hbar\omega/k_B T} - 1)^{-1}$ is the thermal distribution of vibrational occupations, $\Omega \sim 165$ meV is the highest vibrational frequency of diamond, and $\delta(\omega)$ is the average vibrational frequency difference between the electronic states,

TABLE I. Parameters of expression (6) for the temperature shifts of the NV^- visible, infrared, and spin resonances. Only the quadratic electron-phonon interaction parameters (b_4, b_5) were free parameters in the least-squares fits depicted in Fig. 2. The thermal expansion parameters e_i are derived from Ref. [33].

Shift (Unit)	A $\frac{\text{Unit}}{\text{GPa}}$	$\frac{ABe_1}{2}$ Unit/T^2	$\frac{ABe_2}{3}$ Unit/T^3	$\frac{ABe_3}{4}$ Unit/T^4	$\frac{ABe_4}{5}$ Unit/T^5	b_4 Unit/T^4	b_5 Unit/T^5
ΔD (MHz)	14.6[a]	39.7×10^{-7}	-91.6×10^{-9}	70.6×10^{-11}	-60.0×10^{-14}	$18.7(4) \times 10^{-10}$	$-41(2) \times 10^{-13}$
ΔE_V (meV)	5.75[a]	15.6×10^{-7}	-36.1×10^{-9}	27.9×10^{-11}	-23.7×10^{-14}	$8.0(8) \times 10^{-10}$	$-14(3) \times 10^{-13}$
ΔE_{IR} (meV)	1.45[b]	3.95×10^{-7}	-9.12×10^{-9}	7.03×10^{-11}	-5.97×10^{-14}	$1.9(7) \times 10^{-11}$	$-3(1) \times 10^{-15}$

[a]Reference [32].
[b]Reference [1].

which is defined by

$$\delta(\omega)\rho(\omega) = \sum_{\alpha:\omega_{1,\alpha}=\omega} (\omega_{1,\alpha} - \omega_{2,\alpha}) \approx \frac{1}{2\omega} \sum_{\alpha:\omega_{1,\alpha}=\omega} \frac{\partial^2 \Delta E_{el}}{\partial Q_\alpha^2}\bigg|_0 . \tag{5}$$

In the above, Q_α and $\omega_{i,\alpha}$ are the mass-weighted displacement coordinate and frequency of the αth mode in the ith electronic state, respectively, the derivative is evaluated at $Q_\alpha = 0$, and the sum is over all modes with frequency $\omega_{1,\alpha} = \omega$ [31]. The total temperature shift of the ZPL is finally $\Delta E(T) = -\Delta E_{ex}(T) - \Delta E_{e-p}(T)$.

The hydrostatic pressure shifts A of the NV^- visible, infrared, and spin resonances have been previously measured (see Table I) [1,28,32]. So has the volume thermal expansion coefficient of diamond, which can be expressed as a power series $e(T) = \sum_{i=1}^4 e_i T^i$ terminating at T^4 for $T < 300$ K [33]. Importantly, the thermal expansion coefficient depends on the purity of the diamond [33], which is discussed later. Consequently, $\Delta E_{ex}(T)$ of each resonance can be predicted from previous experimental results. Given $\Delta E_{ex}(T)$, $\Delta E_{e-p}(T)$ may be approximately determined for each resonance by first expanding $\delta(\omega)\rho(\omega) \approx \sum_{i=3} a_i \omega^i$, which via the evaluation of the integral in $\Delta E_{e-p}(T)$, yields the temperature expansion $\Delta E_{e-p}(T) \approx \sum_{i=4} b_i T^i$ [31]. The expansion of $\delta(\omega)\rho(\omega)$ commences at ω^3 because as $\omega \to 0$, $\rho(\omega) \propto \omega^2$ (i.e., the Debye density) and for quadratic electron-phonon interactions $\delta(\omega) \propto \omega$ [28,34]. Terminating the expansion of $\Delta E_{e-p}(T)$ at T^5, the approximate expression for a temperature shift is

$$\Delta E(T) \approx -\frac{e_1}{2}ABT^2 - \frac{e_2}{3}ABT^3 - \left(b_4 + \frac{e_3}{4}AB\right)T^4$$
$$- \left(b_5 + \frac{e_4}{5}AB\right)T^5. \tag{6}$$

Note that the expansion of $\Delta E_{e-p}(T)$ has been terminated at T^5 in the above because it was found in fitting the experimental data that termination at T^4 did not yield a satisfactory fit and termination at T^6 did not significantly decrease the fit error.

In our experiments, we employed optical spectroscopy and ODMR techniques to measure the shifts of NV^- ensemble resonances over the temperature range 5–300 K (see Supplemental Material [31]). The shifts of the visible, infrared, and spin resonances were measured in bulk high-pressure high-temperature (HPHT) type Ib samples containing similar nitrogen impurity (40–60 ppm). The shift of the spin resonance was also measured in another bulk HPHT sample with

lower nitrogen impurity (0.4–4 ppm). While the visible and infrared ZPLs were observed in emission, their respective emitting electronic levels are sufficiently long lived for thermal equilibrium of their vibrational levels to be achieved within their lifetime [1]. Figure 2 depicts our observations together with fits using (6) and the shifts $\Delta E_{ex}(T)$ predicted purely by thermal expansion (see Table I for fit parameters). For the shift of D, it is clear that at their respective powers of T, the parameters of $\Delta E_{e-p}(T)$ are an order of magnitude larger than the parameters of $\Delta E_{ex}(T)$, which demonstrates that electron-phonon interactions are necessary to explain the shift.

The NV^- electronic model can be applied to gain further physical insight (see Supplemental Material). Equations (2)
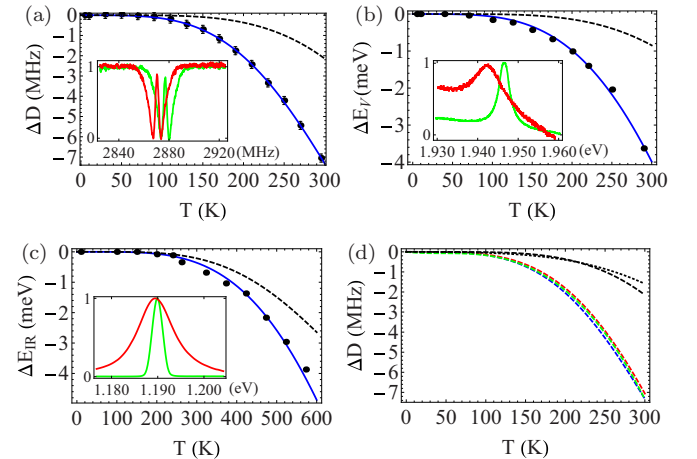

FIG. 2. (Color online) (a)–(c) The temperature shifts of the NV^- spin, visible, and infrared resonances, respectively [black points: measurements; blue curves: fit obtained using (6)]. The contributions of thermal expansion $\Delta E_{ex}(T)$ to each shift alone are depicted as dashed black curves. Experimental uncertainties are discussed in the Supplemental Material. Insets: Example ODMR and photoluminescence spectra (normalized to peak intensity) of the resonances at 5 K (green) and room temperature (red). (d) Comparison of the observed spin resonance shifts in bulk diamonds with different impurity nitrogen concentration [N]: green dashed, [N] < 1 ppm (observed by Chen *et al.* [11]); blue dashed, [N] ∼ 0.4–4 ppm; and red dashed, [N] ∼ 40–60 ppm. The thermal expansion contribution to the spin resonance shift calculated using the thermal expansion coefficients of bulk diamonds with different nitrogen concentration [33]: black dashed: very low concentration, black dotted: high concentration [N] ∼ 78 ppm.

and (5) demonstrate that the thermal expansion and electron-phonon contributions to the ZPL temperature shifts are determined by the first and second derivatives of the electronic energy differences $\Delta E_{\rm el}$ with respect to nuclear displacement. As the nuclei are displaced, the electron-nucleus electrostatic interactions are modified, resulting in changes of the center's orbitals and their energies. The changes to the orbitals in turn perturb electron-electron interactions. The $^3A_2(a_1^2e^2) \to {}^3E(a_1e^3)$ transitions of the visible ZPL involve a change in electronic configuration. Thus, the temperature shift of the visible ZPL depends on how defect orbital energies as well as electron-electron electrostatic repulsion vary with nuclear displacement. The $^1E(a_1^2e^2) \to {}^1A_1(a_1^2e^2)$ transitions of the infrared ZPL and spin transitions of the $^3A_2(a_1^2e^2)$ ground state, however, do not involve a change in electronic configuration, and thus only depend on how electron-electron electrostatic repulsion and spin-spin interaction, respectively, vary with nuclear displacement. Given previous study of the visible ZPL [28], we will concentrate on the temperature shifts of the infrared ZPL and D.

Picturing the defect orbitals as linear combinations of atomic orbitals, nuclear displacement changes the defect orbitals in two ways: (1) the atomic orbitals are displaced, and (2) the linear combinations are modified in response to changed electrostatic interactions [32]. The NV$^-$ molecular model [21,22,35] yields the following expressions for the electronic energy differences $\Delta E_{\rm el}$ of the infrared and spin resonances:

$$\Delta E_{\rm el}^{\rm IR} = 2K\langle e_x(\vec{r}_1)e_y(\vec{r}_2)|\frac{1}{r_{12}}|e_y(\vec{r}_1)e_x(\vec{r}_2)\rangle \approx \frac{K}{3}\eta^2\left\langle\frac{1}{r_{12}}\right\rangle,$$

$$D = C\langle e_x(\vec{r}_1)e_y(\vec{r}_2)|\frac{1}{r_{12}^3} - \frac{3z_{12}^2}{r_{12}^5}[|e_x(\vec{r}_1)e_y(\vec{r}_2)\rangle \qquad (7)$$

$$-|e_y(\vec{r}_1)e_x(\vec{r}_2)\rangle] \approx C\eta^2\left\langle\frac{1}{r_{12}^3} - \frac{3z_{12}^2}{r_{12}^5}\right\rangle,$$

where K and C are the electron-electron electrostatic and spin-spin interaction constants (see Supplemental Material for definition), respectively, $\vec{r}_i = x_i\hat{\vec{x}} + y_i\hat{\vec{y}} + z_i\hat{\vec{z}}$ is the position of the ith electron, $r_{12} = |\vec{r}_2 - \vec{r}_1|$, $z_{12} = z_2 - z_1$, $\langle\cdots\rangle = \langle c_1(\vec{r}_1)c_2(\vec{r}_2)|\cdots|c_1(\vec{r}_1)c_2(\vec{r}_2)\rangle$, c_i are the dangling sp^3 atomic orbitals of the vacancy's three nearest-neighbor carbon atoms, and $\eta = \sum_{i=1}^3 |\langle c_i|e_x\rangle|^2 \sim 0.84$ [17]. The approximations in

the above are the neglect of atomic orbitals other than those of the three nearest-neighbor carbon atoms and the neglect of orbital overlaps. The expressions highlight two factors: (1) the electron density η associated with the three carbon atoms and (2) the expectation value of the interaction between the dangling sp^3 electron densities of two of the carbon atoms. As defined in (2) and (5), the parameters of Table I are directly related to the first and second derivatives of these factors with nuclear displacement. These parameters therefore provide insight into how the electron density and interaction expectation values depend on nuclear displacement. Future *ab initio* calculations of these parameters will yield further insight into the center's vibronic properties.

The principal implication for NV$^-$ metrology that our model reveals concerns the variation of $\Delta D(T)$ between nanodiamond NV$^-$ centers. If $\Delta D(T)$ varies significantly between each nanodiamond NV$^-$ thermometer, then the implementation of NV$^-$ nanothermometry is potentially inhibiting by the necessity for either careful fabrication of consistent NV$^-$ thermometers or the calibration and marking of each NV$^-$ thermometer. The possible sources of variation in nanodiamond are structural defects, impurities, strain, and surface morphology. Each of these will predominately affect the thermal expansion coefficient. As an example, Fig. 2(d) compares the reported $\Delta D(T)$ and calculated $\Delta E_{\rm ex}(T)$ contribution of centers in bulk diamonds with different nitrogen impurity. Figure 2(d) demonstrates that while the thermal expansion contributions differ significantly between diamonds with different nitrogen impurity, the observed $\Delta D(T)$ are very similar. This outcome is due to the dominant contribution of $\Delta E_{\rm e-p}(T)$ to $\Delta D(T)$, which varies little with nitrogen impurity. Only in very small nanodiamonds or very high impurity, where the density $\rho(\omega)$ of vibrational modes is modified, will the contribution of $\Delta E_{\rm e-p}(T)$, and thus $\Delta D(T)$, vary significantly. Hence, the dominant contribution of electron-phonon interactions to $\Delta D(T)$ is promising for the implementation of NV$^-$ nanothermometry.

[1] M. W. Doherty, N. B. Manson, P. Delaney, F. Jelezko, and L. C. L. Hollenberg, Phys. Rep. **528**, 1 (2013).

[2] F. Dolde, H. Fedder, M. W. Doherty, T. Nöbauer, F. Rempp, G. Balasubramanian, T. Wolf, F. Reinhard, L. C. L. Hollenberg, F. Jelezko, and J. Wrachtrup, Nat. Phys. **7**, 459 (2011).

[3] S. Hong, M. S. Grinolds, L. M. Pham, D. Le Sage, L. Luana, R. L. Walsworth, and A. Yacoby, MRS Bull. **38**, 155 (2013).

[4] M. S. Grinolds, S. Hong, P. Maletinsky, L. Luan, M. D. Lukin, R. L. Walsworth, and A. Yacoby. Nat. Phys. **9**, 215 (2013).

[5] H. J. Mamin, M. Kim, M. H. Sherwood, C. T. Rettner, K. Ohno, D. D. Awschalom, and D. Rugar, Science **339**, 557 (2013).

[6] T. Staudacher, F. Shi, S. Pezzagna, J. Meijer, J. Du, C. A. Meriles, F. Reinhard, and J. Wrachtrup, Science **339**, 561 (2013).

[7] L. P. McGuinness, Y. Yan, A. Stacey, D. A. Simpson, L. T. Hall, D. Maclaurin, S. Prawer, P. Mulvaney, J. Wrachtrup, F. Caruso, R. E. Scholten, and L. C. L. Hollenberg, Nat. Nanotechnol. **6**, 358 (2011).

[8] V. M. Acosta, E. Bauch, M. P. Ledbetter, A. Waxman, L.-S. Bouchard, and D. Budker, Phys. Rev. Lett. **104**, 070801 (2010).

[9] D. M. Toyli, D. J. Christle, A. Alkauskas, B. B. Buckley, C. G. Van de Walle, and D. D. Awschalom, Phys. Rev. X **2**, 031001 (2012).

[10] V. M. Acosta, A. Jarmola, L. J. Zipp, M. P. Ledbetter, E. Bauch, and D. Budker, Proc. SPIE **7948**, 79480W (2011).

[11] X.-D. Chen, C.-H. Dong, F.-W. Sun, C.-L. Zou, J.-M. Cui, Z.-F. Han, and G.-C. Guo, Appl. Phys. Lett. **99**, 161903 (2011).

[12] D. M. Toyli, C. F. de las Casas, D. J. Christle, V. V. Dobrovitski, and D. D. Awschalom, Proc. Natl. Acad. Sci. USA **110**, 8417 (2013).

[13] P. Neumann, I. Jakobi, F. Dolde, C. Burk, R. Reuter, G. Waldherr, J. Honert, T. Wolf, A. Brunner, J. H. Shim, D. Suter, H. Sumiya, J. Isoya, and J. Wrachtrup, Nano Lett. **13**, 2738 (2013).

[14] G. Kucsko, P. C. Maurer, N. Y. Yao, M. Kubo, H. J. Noh, P. K. Lo, H. Park, and M. D. Lukin, Nature (London) **500**, 54 (2013).

[15] K. Fang, V. M. Acosta, C. Santori, Z. Huang, K. M. Itoh, H. Watanabe, S. Shikata, and R. G. Beausoleil, Phys. Rev. Lett. **110**, 130802 (2013).

[16] X.-F. He, N. B. Manson, and P. T. H. Fisk, Phys. Rev. B **47**, 8816 (1993).

[17] S. Felton, A. M. Edmonds, M. E. Newton, P. M. Martineau, D. Fisher, D. J. Twitchen, and J. M. Baker, Phys. Rev. B **79**, 075203 (2009).

[18] J. A. Larsson and P. Delaney, Phys. Rev. B **77**, 165201 (2008).

[19] A. Gali, M. Fyta, and E. Kaxiras, Phys. Rev. B **77**, 155206 (2008).

[20] F. M. Hossain, M. W. Doherty, H. F. Wilson, and L. C. L. Hollenberg, Phys. Rev. Lett. **101**, 226403 (2008).

[21] M. W. Doherty, N. B. Manson, P. Delaney, and L. C. L. Hollenberg, New J. Phys. **13**, 025019 (2011).

[22] J. R. Maze, A. Gali, E. Togan, Y. Chu, A. Trifonov, E. Kaxiras, and M. D. Lukin, New J. Phys. **13**, 025025 (2011).

[23] G. Davies and M. F. Hamer, Proc. R. Soc. London, Ser. A **348**, 285 (1976).

[24] L. J. Rogers, S. Armstrong, M. J. Sellars, and N. B. Manson, New J. Phys. **10**, 103024 (2008).

[25] V. M. Acosta, A. Jarmola, E. Bauch, and D. Budker, Phys. Rev. B **82**, 201202(R) (2010).

[26] N. Manson, L. Rogers, M. Doherty, and L. Hollenberg, arXiv:1011.2840.

[27] J. H. N. Loubser and J. A. van Wyk, Rep. Prog. Phys. **41**, 1201 (1978).

[28] G. Davies, J. Phys. C: Solid State Phys. **7**, 3797 (1974).

[29] A. T. Collins, M. F. Thomaz, and M. I. B. Jorge, J. Phys. C: Solid State Phys. **16**, 2177 (1983).

[30] T. Plakhotnik and D. Gruber, Phys. Chem. Chem. Phys. **12**, 9751 (2010).

[31] See Supplemental Material at http://link.aps.org/supplemental/10.1103/PhysRevB.90.041201 for experimental details and detailed discussion of the temperature shift model.

[32] M. W. Doherty, V. V. Struzhkin, D. A. Simpson, L. P. McGuinness, Y. Meng, A. Stacey, T. J. Karle, R. J. Hemley, N. B. Manson, L. C. L. Hollenberg, and S. Prawer, Phys. Rev. Lett. **112**, 047601 (2014).

[33] T. Sato, K. Ohashi, T. Sudoh, K. Haruna, and H. Maeta, Phys. Rev. B **65**, 092102(R) (2002).

[34] A. A. Maradudin, Solid State Phys. **18**, 274 (1966).

[35] M. W. Doherty, F. Dolde, H. Fedder, F. Jelezko, J. Wrachtrup, N. B. Manson, and L. C. L. Hollenberg, Phys. Rev. B **85**, 205203 (2012).